*Title Page (including paper title & Complete corresponding author details)

Title:
Prospective intra-individual comparison of standard dose versus reduced-dose thoracic CT using hybrid and pure iterative reconstruction in a follow-up cohort of pulmonary nodules – Effect of detectability of pulmonary nodules with lowering dose based on nodule size, type and body mass index.

Authors' full names:
Dr Varut Vardhanabhuti FRCR [1,2]
Dr Chun-Lap Pang FRCR [1,3]
Dr Sean Tenant FRCR [3]
Dr James Taylor FRCR [3]
Professor Christopher Hyde FRCP [4]
Professor Carl Roobottom FRCR [1,3]

Affiliations:
1. Plymouth University Peninsula Schools of Medicine and Dentistry, John Bull Building, Plymouth, PL6 8BU, United Kingdom
2. Department of Diagnostic Radiology, Li Ka Shing Faculty of Medicine, University of Hong Kong, Hong Kong
3. Department of Radiology, Derriford Hospital, Derriford Road, Plymouth, PL6 8DH, United Kingdom
4. University of Exeter Medical School, Exeter, United Kingdom

Corresponding Author:
Dr Varut Vardhanabhuti
Department of Diagnostic Radiology, Li Ka Shing Faculty of Medicine, University of Hong Kong, Room 406, Block K, Queen Mary Hospital, Pok Fu Lam Road, Hong Kong
Email: varv@hku.hk
Tel: +852 2254524
Fax: +852 28551652

Title:

Prospective intra-individual comparison of standard dose versus reduced-dose thoracic CT using hybrid and pure iterative reconstruction in a follow-up cohort of pulmonary nodules – Effect of detectability of pulmonary nodules with lowering dose based on nodule size, type and body mass index.

Abbreviations:

FBP - filtered back projection

ASIR- adaptive statistical reconstruction

MBIR - model-based iterative reconstruction

STD - standard dose

RD1 – reduced dose 1

RD2 – reduced dose 2

ABSTRACT

Objectives

To determine the diagnostic accuracy of lung nodule detection in thoracic CT using 2 reduced dose protocols comparing 3 available CT reconstruction algorithms (filtered back projection-FBP, adaptive statistical reconstruction-ASIR and model-based iterative reconstruction-MBIR) in a western population.

Materials and Methods:

A prospective single-center study recruited 98 patients with written consent. Standard dose (STD) thoracic CT followed by 2 reduced-dose protocols using automatic tube current modulation (RD1) and fixed tube current (RD2) were performed and reconstructed with FBP, ASIR and MBIR with subsequent diagnostic accuracy analysis for nodule detection.

Results:

108 solid nodules, 47 subsolid nodules and 89 purely calcified nodules were analyzed. RD1 was superior to RD2 for assessment of solid nodules ≤4mm, and subsolid nodules ≤5mm ($p<0.05$). Deterioration of RD2 is correlated to patient's body mass index and least affected by MBIR. For solid nodules ≤4mm, MBIR area under curve (AUC) for RD1 was 0.935/0.913 and AUC for RD2 was 0.739/0.739, for rater 1/rater2 respectively. For subsolid nodules ≤5mm, MBIR AUC for RD1 was 0.971/0.986 and AUC for RD2 was 0.914/0.914, for rater 1/rater2 respectively. For calcified nodules excellent detection accuracy was maintained regardless of reconstruction algorithms with AUC >0.97 for both readers across all dose and reconstruction algorithms.

Conclusions:

Diagnostic performance of lung nodule is affected by nodule size, protocol, reconstruction algorithm and patient's body habitus. The protocol in this study showed that RD1 was superior to RD2 for assessment of solid nodules ≤4mm, and subsolid nodules ≤5mm and deterioration of RD2 is related to patient's body mass index.

Introduction:

There is evidence that in selected high-risk individuals, low dose computed tomography (LDCT) screening significantly reduces lung cancer mortality and all-cause mortality and is recommended by many international organizations [1, 2]. However, as outlined by the recent Cochrane review, the relative harms and benefits of screening across different risk groups and settings needs to be considered and there is a requirement for standardized practices for screening with LDCT [3, 4]. The ACR–Society of Thoracic Radiology suggests CT examinations should be acquired by using multidetector scanners with at least 16 detector rows, a helical technique, and with the patient in a suspended state of full inspiration [5]. For a standardized patient, it is recommended that the technique should deliver CTDIvol of ≤3mGy. To maximize the risk-benefit ratio in favor of the screened individual, the radiation dose should be as low as reasonably achievable without compromising image quality and accurate detection but the maximum extent of dose reduction has not yet been established. The broad availability of iterative reconstruction algorithms on clinical CT scanners has enabled significant potential dose reduction in the context of screening. There are several versions of iterative reconstructions. The first generation (hybrid) shows dose reduction in the range of 30-40% [6-11]. The second generation iterative reconstruction (pure) has shown more dose reduction capability with reported range of 50-80% compared to the traditional filtered-back projection (FBP) [12-17]. Recent papers have explored the feasibility of using 'pure' iterative reconstruction e.g. model-based iterative reconstruction (MBIR) in the context of lung nodule surveillance [18-20]. It has been shown that it is possible to achieve meaningful image quality but significant dose reduction was achieved on selected patients with low body weight or BMI. In a western population, the average body weight/BMI are considerably higher. Currently, there are 2 broad strategies in performing LDCT with regards to setting of tube current. Investigators have used either tube current modulation approach or

a fixed tube current approach. It is not clear which methods are more reliable in real world setting where there is large variation in body size.

The purpose of our study is to determine the diagnostic accuracy of lung nodule detection in thoracic CT using 2 reduced dose protocols using automatic tube current modulation and fixed tube current approaches comparing 3 available CT reconstruction algorithms (filtered back projection-FBP, adaptive statistical reconstruction-ASIR and model-based iterative reconstruction-MBIR) to reference standard-dose thoracic CT in a western population.

Materials and Methods

Study Population

This prospective single-center study obtained institutional review board approval and recruited 98 patients. Patients were identified from referral to department for a non-contrast CT Thorax with a specific indication of follow-up of previously detected lung nodule(s) on a prior CT scan. The identified participants were interviewed and on agreement were prospectively enrolled consecutively from August 2013 – February 2015. Written informed consent was obtained on all patients. We follow the previously published Fleischner society guidelines for follow-up of solitary pulmonary nodule [21, 22].

Inclusion and Exclusion criteria

Inclusion criteria for the study were as follows: age more than or equal to 40 years of age at the time of scan, able to provide informed written consent, able to hold their breath for at least 20 seconds, able to follow verbal commands for breath holding and remain still for the duration of scanning, able to put arms over head for the entirety of the scan. Exclusion criteria were as follows: unable to give inform consent, other scan indication (e.g. with contrast, CT pulmonary angiogram, etc), unable to put hands over their head. Patient demographics (weight, height, and body mass index (calculated by weight / height in meters square) and clinical information (e.g. previous thoracic surgery, history of malignancy, clinical symptoms) were recorded.

Imaging Parameters

All examinations were performed with a 64-row detector CT scanner (Discovery 750 HD; GE Healthcare, Wisconsin, USA). No intravenous contrast was given. Standard dose scan parameters were as follows: tube voltage 120, rotation time 0.5s, pitch 1.375:1, noise index 39.6, tube current range 10-750mA. Reduced-dose 1 (RD1) scan parameters were as follows:

tube voltage 100, rotation time 0.5s, pitch 1.375:1, noise index 85, tube current range 10-750mA. Reduced-dose 2 (RD2) scan parameters were as follows: tube voltage 100, rotation time 0.5s, pitch 0.984:1, fixed tube current 10mA. All Patients were scanned in a single breath-hold.

Scanning Parameters

The order of 2 reduced dose scans were randomized after the initial standard of care scan to even out the effect of artefact that could inadvertently occur if the patient breathed during scanning. It is thought that this would be more likely to occur towards the end of the scan. Block randomization method was used to maintain equal numbers in each arm.

Reconstruction Algorithms

All patients received 3 scans in total (STD, RD1 and RD2). Each scan was reconstructed with FBP, ASIR with 30% blending, and MBIR. For each patient, this generated 9 scans and for all patients this generated a total of 882 scans. For the purpose of assessment, standard dose with ASIR was used as reference standard because in our center this is in routine clinical use, and our standard dose protocol are already optimized for ASIR not FBP. The remaining scans and reconstruction algorithms serve as index tests under evaluation (see Figure 1).

Radiation Dose

DLP and CTDIvol were recorded for each scanning series. AP and lateral diameters were recorded and by using the conversion factors as per American Association of Physicists Medicine (AAPM) guidelines, SSDE was calculated [23]. Effective doses (ED) were also estimated using a conversion of 0.014 taken from a normalized value of ED per DLP for chest [24].

Objective Image Assessment

Quantitative measurements were performed using advanced open-source PACS workstation DICOM viewer (Osirix 3.8.1 on Mac OS, Pixmeo, Geneva, Switzerland) and GE (GE Healthcare, Wisconsin, USA) Workstations with dedicated Volume Viewer (v.4.6). Mean CT attenuation values (in Hounsfield units) and standard deviation were obtained in three consecutive images over the aorta by manually placing a circular region on interests (ROIs) which were duplicated to all 9 series. ROIs were copied to identical slices to allow for accurate comparison between different dose scans in the same patient at same location. For each study, the image noise was measured as the standard deviation of the pixel values drawn over the aorta. Signal to noise ratio was calculated by dividing mean HU by mean SD.

Subjective Image Assessment

All image data sets were assessed blinded and randomized manner by two experienced thoracic radiologists (5 and 8 years' experience) separately. Mean scores were calculated for each of the reconstructed series. Subjective image quality were assessed in terms of subjective image noise, subjective image contrast, artifacts and diagnostic confidence.

Subjective analysis scoring criteria

Subjective image noise was assessed using a five-point scale (1 = unacceptable image noise, 2 = above average noise, 3 = average image noise, 4 = less than average noise, and 5 = minimal image noise).

Image contrast was assessed by using a five-point scale (1= very poor contrast, 2 = suboptimal image contrast, 3 = acceptable image contrast, 4 = above average contrast, and 5 = excellent image contrast).

Diagnostic confidence was assessed by using a four-point scale (1 = poor confidence, 2 = confident only for a limited clinical entity such as a calcified lesion, or a large lesion, 3 = probably confident, and 4 = completely confident). Scores for diagnostic confidence was used

to subsequently calculate a cut-off threshold for images that were adequate for diagnosis. Scores of 1 and 2 were classified as non-diagnostic and scores of 3 and 4 were classified as of diagnostic quality.

Diagnostic Accuracy

For the diagnostic accuracy assessment, the primary endpoint was the presence or absence of pulmonary nodules. The readers were asked to record the presence/absence of nodules per lobe basis. The types of nodules were classified as solid (including predominantly solid nodule with mixed density containing fat or calcification), purely calcified, or subsolid. One reader was asked to view all reconstruction side-by-side, with available clinical information and reporting viewed subsequently for consensus with a second reader. This then acted as reference standard. Size (as average of length and width) were measured and based on classification of Fleischner society. For solid nodules, they were classified into 4 categories as follows: ≤4mm, 4.1-5.9mm, 6-7.9mm and ≥8mm. For subsolid, measurements were averaged over the largest diameter of ground glass components and were classified into 2 categories as follows: ≤5mm and >5mm. For purely calcified nodules, readers were asked to identify only nodules ≥4mm. Two separate readers (8 and 20 years' experience) subsequently were asked to read the blinded scans one at a time for the purpose of diagnostic accuracy in nodule detection. This was done in 18 separate reporting sessions of at least 1 week apart to avoid recall bias. Area under curve for each types of nodules were then calculated compared with reference standard for each types of nodules, on a per lobe basis. Readers were allowed to adjust windowing and use maximum intensity projection as per normal clinical reporting practice. No computer aided detection software was used.

Statistical Analysis

Data were analyzed with a statistical software package (Stata 13.1, Stata Corp, Texas, USA). Sample size was calculated using 2-tail t-test linear regression model based on 97% power, effect size of 0.15 and α-probability of 0.05 giving sample size of 98. Quantitative image metrics such as objective image noise and CT numbers using analysis of variance (ANOVA). Friedman's test with Dunn's multiple comparison was used to analyze subjective image quality and other qualitative lesion assessment parameters. Interobserver variability was compared using kappa statistics. Grading was classified as follows: 0.21 – 0.40: fair agreement; 0.41 – 0.60: moderate agreement, 0.61 – 0.80: substantial agreement, 0.81 – 1.00: almost perfect agreement. Diagnostic accuracy was calculated by area under curve (AUC), with sensitivity and specificity calculated for nodule detection using ASIR standard dose as reference. A p-value of <0.05 was considered statistically significant.

Results

Patient demographics are listed in Table 1. There were 62 men and 38 women. Mean age was 66.2 (range 43-89). Mean BMI was 28.2 (± 6.5 SD). Radiation dose is listed in Table 2. DLP were 235.5, 68.7 and 9.9 mGy.cm for STD, RD1 and RD2 respectively. SSDE were 7.4, 2.1 and 0.3 mGy for STD, RD1 and RD2 respectively.

Objective Image Assessment

There was significant difference between the measured noise across all reconstruction algorithms and dose. Compared to standard dose ASIR, FBP shows higher image noise, and MBIR shows lower image noise ($p<0.05$). This is tabulated in Table 3. In terms of attenuation values, compared to standard dose ASIR, no significant difference exists between different doses and algorithms except for RD2 MBIR ($p<0.05$). This is tabulated in Table 4. We postulate that the reduced mean attenuation values for RD2 MBIR may be due to over correction of an otherwise noisy raw images obtained from very low dose scan.

Subjective Image Assessment

ASIR STD had the best mean scores but no statistical differences between FBP STD and MBIR STD ($p>0.05$). Statistical significantly poorer scores were seen for reduced dose scans across all reconstructions ($p<0.05$). The scores were worse for RD2 compared to RD1. For reduced dose scans, FBP had the worse score compared to other reconstruction algorithms ($p<0.05$). For RD1, MBIR was superior to ASIR ($p<0.05$). For RD2, MBIR and ASIR were not significantly different ($p>0.05$). For representative images, refer Figure 2-3. Results are tabulated in Table 5. Interobserver agreement ranged from moderate to almost perfect ($k=$ 0.54-0.81 for subjective image noise; $k=0.65$-0.89 for subjective image contrast; $k=$ 0.54-0.89 for diagnostic confidence). Diagnostic confidence was further analyzed to identify studies that were deemed of diagnostic quality This shows that there is reduced diagnostic

acceptability for RD2, and to lesser extent RD1. The diagnostic acceptability was 100% for STD dose (FBP, ASIR, MBIR), RD1 (MBIR). This reduced to 98% for RD 1 (ASIR and FBP), 91.8% for RD2 (ASIR and MBIR, and most reduced to 85.7% for RD2 (FBP).) The reduced quality was correlated to patients with high BMI (see Figure 4-5).

Diagnostic Accuracy

AUC, sensitivity and specificity were calculated and overall detection accuracy is shown in Table 6. Further sub-analysis based on lesion size for solid and subsolid nodules were also performed and is shown in Table 7-8. The inter-observer agreement was almost perfect and was 0.971, 0.973 and 0.981 respectively for solid, subsolid and calcified nodules.

Solid Nodules:

There were a total of 108 solid nodules (≤4mm: 23, 4.1-5.9mm: 36, 6-7.9mm: 25, ≥8mm: 24). For solid nodules, excellent detection accuracy was maintained when using standard dose regardless of reconstruction algorithms with AUC >0.98 for both readers. For ASIR, AUC for RD1 was 0.977/0.963 and AUC for RD2 was 0.917/0.916, respectively for rater 1/rater2. For FBP, AUC for RD1 was 0.958/0.944 and AUC for RD2 was 0.856/0.841, respectively for rater 1/rater2. For MBIR, AUC for RD1 was 0.972/0.958 and AUC for RD2 was 0.921/0.916, respectively for rater 1/rater2. The detection of nodules were significantly impaired for nodules of <4mm (see Figure 6). This was markedly worse for RD2. For ASIR, AUC for RD1 was 0.935/0.913 and AUC for RD2 was 0.717/0.717, respectively for rater 1/rater2. For FBP, AUC for RD1 was 0.913/0.891 and AUC for RD2 was 0.609/0.587, respectively for rater 1/rater2. For MBIR, AUC for RD1 was 0.935/0.913 and AUC for RD2 was 0.739/0.739, respectively for rater 1/rater2. For nodules >4.1mm, detection accuracy was maintained at AUC > 0.95 in all cases except for FBP reconstruction of RD1 and RD2.

Subsolid Nodules:

There were a total of 47 subsolid nodules (≤5mm: 35, >5.1mm: 12). For subsolid nodules, excellent detection accuracy was maintained when using standard dose regardless of reconstruction algorithms with AUC >0.98 for both readers. For ASIR, AUC for RD1 was 0.979/0.988 and AUC for RD2 was 0.936/0.935, respectively for rater 1/rater2. For FBP, AUC for RD1 was 0.947/0.956 and AUC for RD2 was 0.894/0.883, respectively for rater 1/rater2. For MBIR, AUC for RD1 was 0.979/0.988 and AUC for RD2 was 0.936/0.935, respectively for rater 1/rater2.

The detection of subsolid nodules were mildly impaired for size of <5mm for RD2. For ASIR, AUC for RD1 was 0.971/0.986 and AUC for RD2 was 0.914/0.914, respectively for rater 1/rater2. For FBP, AUC for RD1 was 0.929/0.943 and AUC for RD2 was 0.857/0.843, respectively for rater 1/rater2. For MBIR, AUC for RD1 was 0.971/0.986 and AUC for RD2 was 0.914/0.914, respectively for rater 1/rater2. For size >5mm, detection accuracy was maintained at AUC > 0.99 in all cases.

Purely Calcified Nodules:

There were a total of 89 purely calcified nodules. For calcified nodules excellent detection accuracy was maintained regardless of reconstruction algorithms with AUC >0.97 for both readers across all dose and reconstruction algorithms.

Analysis according to BMI

Loss of nodule detection, that was seen in reduced dose scans was further sub classified according to patient's BMI. Loss of detection was defined if one or more rater did not spot the nodule and this was related to BMI. For RD1, loss of detection was seen in the 2 largest patients (BMI 52.4 and 54.7) but only for FBP and ASIR. For RD2 loss of detection was seen in 8 largest patients (BMI 38.6-54.7) for ASIR and MBIR and in 12 patients (BMI 32.4-54.7) for FBP.

Discussion

Diagnostic performance of lung nodule is affected by nodule size, protocol, reconstruction algorithm and patient's body habitus. The protocol in this study showed that RD1 was superior to RD2 for assessment of solid nodules ≤4mm, and subsolid nodules ≤5mm and deterioration of RD2 is related to patient's body mass index. It is important to be aware that in pursuit of low dose, one must not compromise on diagnostic quality. Recent study in chest phantom examining detectability of lung nodule at chest radiograph equivalent dose has shown overall detection rates of 93.3% with DLP: 9mGy*cm [25]. Their detection rates for small 5mm solid nodules were 83.9 % using iterative reconstruction. The dose in this study was similar to our RD2 protocol dose. Our results demonstrate slightly poorer performance but this can be explained by the fact that we performed on real patients, many of whom have larger body size compared to the phantom model. Several previous studies have been performed using ultra low dose chest CT but scanning in 'standard sized' western patient has not been extensively tested [17, 18, 20, 26, 27]. It is known that iterative reconstruction may cause impairment in subjective image quality especially at very low doses [26] and is in line with our subjective analysis findings. In our study, the main focus was on the detection of nodules in a follow-up cohort. Inclinical practice, one must be acutely aware of the effect of patient's body size on detection accuracy. For both reduced dose approaches, we have shown that there are limits to how far once can reduce the dose. The diagnostic acceptability for nodule detection subjectively was reduced when tube current modulation approach was used at BMI > 52, whereas for the fixed approach this was at BMI > 38. This is further confirmed when loss of nodule detection was further subclassified based on BMI. These BMIs appear to be the rough estimation of ceiling limits for both approaches in our study, but it must be noted that only small number of patients were scanned in our study with high BMI (BMI>50: n=2; BMI>38: n=8). Further studies with more patients at high BMI range will be required to

reach proper conclusion. In further analysis based on nodule size, we have shown that the accuracy is impaired mostly in solid nodules of ≤4mm. Accuracy for solid nodules > 4.1mm, subsolid nodules, and purely calcified nodules have AUC > 0.91. The exception is FBP RD2 for ≤ 5mm subsolid nodules where AUC is 0.857/0.843. The reason for this may be that the detection of small subsolid nodules is also heavily influenced by increased image noise which is most prominent with FBP RD2. The reduced diagnostic accuracy for solid nodules <4mm is in line with previous findings on a different iterative reconstruction technique at similar dose [28]. By using the RD1, AUCs for FBP and ASIR even for small solid nodules ≤4mm are reasonable with AUC for ASIR RD1 was 0.935/0.913 and FBP RD1 was 0.913/0.891 respectively for each rater. So even for centers without the latest pure iterative reconstruction, one may still be able to achieve significant dose reduction without significant compromise on accuracy. It is important to be aware of the limit of detection accuracy in a technique and clinical indication of a test will determine the level at which one can afford to set a threshold limit. In the context of pulmonary nodule follow-up for suspected pulmonary metastasis in patients who has a history of malignancy, accurate detection is needed regardless of size, as detection no matter how small is likely to lead to change in management. In the context of lung cancer screening, there is now increasing evidence that detection of nodules < 5mm for example from the NELSON trial, no follow up is needed as these nodules are not predictive of lung cancer with low probability similar to individuals without nodules [29]. Therefore in this context, one may rightly choose to obviate the need for detection of small clinically irrelevant nodules.

There are several limitations in our study. First, our gold standard is nodule detected on standard dose ASIR. We have no pathological proof of clinical significance, but for the purpose of diagnostic accuracy study, our gold standard is that of an accepted reference test now in use in routine clinical practice. Second, although studies were analyzed in a blinded

manner, it was noted that MBIR images have unique appearances, so complete blinding was difficult, nevertheless steps were made to present image datasets in a randomized manner and all identifiable information removed. Third, we set out to examine differences between automatic tube current modulation and fixed current approaches. We did not alter protocols based on BMI but results from this work will give guidance to future studies that may incorporate BMI into protocols. Fourth, we acknowledged that the study design requires an increase in radiation exposure to the patient, but the incremental increase was on average around 33% increase from average dose, and this was deemed acceptable from our ethics board of approval.

Conclusion:

In conclusion, we have shown in our study that the detection accuracy will drop significantly if a 'one fits all' approach is used either using the fixed tube current or the tube current modulation approaches. Being aware of the limitation boundary of low dose approaches will ensure that diagnostic accuracy of nodule detection will not be affected which must be based on individual patients and clinical indication as we move our imaging protocols towards the era of personalized medicine. Individualization of CT protocols taking into account detection accuracy limits based on nodule type/size, standard/low dose setting, reconstruction algorithms and patient's size should be encouraged.

Acknowledgements:

None

References:

[1] M.T. Jaklitsch, F.L. Jacobson, J.H. Austin, J.K. Field, J.R. Jett, S. Keshavjee, H. MacMahon, J.L. Mulshine, R.F. Munden, R. Salgia, G.M. Strauss, S.J. Swanson, W.D. Travis, D.J. Sugarbaker, The American Association for Thoracic Surgery guidelines for lung cancer screening using low-dose computed tomography scans for lung cancer survivors and other high-risk groups, The Journal of thoracic and cardiovascular surgery 144(1) (2012) 33-8.
[2] R. Wender, E.T. Fontham, E. Barrera, Jr., G.A. Colditz, T.R. Church, D.S. Ettinger, R. Etzioni, C.R. Flowers, G.S. Gazelle, D.K. Kelsey, S.J. LaMonte, J.S. Michaelson, K.C. Oeffinger, Y.C. Shih, D.C. Sullivan, W. Travis, L. Walter, A.M. Wolf, O.W. Brawley, R.A. Smith, American Cancer Society lung cancer screening guidelines, CA: a cancer journal for clinicians 63(2) (2013) 107-17.
[3] R. Manser, A. Lethaby, L.B. Irving, C. Stone, G. Byrnes, M.J. Abramson, D. Campbell, Screening for lung cancer, The Cochrane database of systematic reviews (6) (2013) Cd001991.
[4] M. Usman Ali, J. Miller, L. Peirson, D. Fitzpatrick-Lewis, M. Kenny, D. Sherifali, P. Raina, Screening for lung cancer: A systematic review and meta-analysis, Preventive medicine (2016).
[5] E.A. Kazerooni, J.H. Austin, W.C. Black, D.S. Dyer, T.R. Hazelton, A.N. Leung, M.F. McNitt-Gray, R.F. Munden, S. Pipavath, ACR-STR practice parameter for the performance and reporting of lung cancer screening thoracic computed tomography (CT): 2014 (Resolution 4), Journal of thoracic imaging 29(5) (2014) 310-6.
[6] J. Leipsic, G. Nguyen, J. Brown, D. Sin, J.R. Mayo, A prospective evaluation of dose reduction and image quality in chest CT using adaptive statistical iterative reconstruction, AJR. American journal of roentgenology 195(5) (2010) 1095-9.
[7] P. Prakash, M.K. Kalra, J.B. Ackman, S.R. Digumarthy, J. Hsieh, S. Do, J.A. Shepard, M.D. Gilman, Diffuse lung disease: CT of the chest with adaptive statistical iterative reconstruction technique, Radiology 256(1) (2010) 261-9.
[8] P. Prakash, M.K. Kalra, S.R. Digumarthy, J. Hsieh, H. Pien, S. Singh, M.D. Gilman, J.A. Shepard, Radiation dose reduction with chest computed tomography using adaptive statistical iterative reconstruction technique: initial experience, Journal of computer assisted tomography 34(1) (2010) 40-5.
[9] F. Pontana, J. Pagniez, T. Flohr, J.B. Faivre, A. Duhamel, J. Remy, M. Remy-Jardin, Chest computed tomography using iterative reconstruction vs filtered back projection (Part 1): Evaluation of image noise reduction in 32 patients, European radiology 21(3) (2011) 627-35.
[10] S. Singh, M.K. Kalra, M.D. Gilman, J. Hsieh, H.H. Pien, S.R. Digumarthy, J.A. Shepard, Adaptive statistical iterative reconstruction technique for radiation dose reduction in chest CT: a pilot study, Radiology 259(2) (2011) 565-73.
[11] H.J. Hwang, J.B. Seo, H.J. Lee, S.M. Lee, E.Y. Kim, S.Y. Oh, J.E. Kim, Low-dose chest computed tomography with sinogram-affirmed iterative reconstruction, iterative reconstruction in image space, and filtered back projection: studies on image quality, Journal of computer assisted tomography 37(4) (2013) 610-7.
[12] L.L. Geyer, U.J. Schoepf, F.G. Meinel, J.W. Nance, Jr., G. Bastarrika, J.A. Leipsic, N.S. Paul, M. Rengo, A. Laghi, C.N. De Cecco, State of the Art: Iterative CT Reconstruction Techniques, Radiology 276(2) (2015) 339-57.
[13] M. Katsura, I. Matsuda, M. Akahane, J. Sato, H. Akai, K. Yasaka, A. Kunimatsu, K. Ohtomo, Model-based iterative reconstruction technique for radiation dose reduction in chest CT: comparison with the adaptive statistical iterative reconstruction technique, European radiology 22(8) (2012) 1613-23.
[14] S.H. Lee, M.J. Kim, C.S. Yoon, M.J. Lee, Radiation dose reduction with the adaptive statistical iterative reconstruction (ASIR) technique for chest CT in children: an intra-individual comparison, European journal of radiology 81(9) (2012) e938-43.
[15] Y. Lee, K.N. Jin, N.K. Lee, Low-dose computed tomography of the chest using iterative reconstruction versus filtered back projection: comparison of image quality, Journal of computer assisted tomography 36(5) (2012) 512-7.
[16] L.P. Qi, Y. Li, L. Tang, Y.L. Li, X.T. Li, Y. Cui, Y.S. Sun, X.P. Zhang, Evaluation of dose reduction and image quality in chest CT using adaptive statistical iterative reconstruction with the same group of patients, The British journal of radiology 85(1018) (2012) e906-11.
[17] V. Vardhanabhuti, R.J. Loader, G.R. Mitchell, R.D. Riordan, C.A. Roobottom, Image quality assessment of standard- and low-dose chest CT using filtered back projection, adaptive statistical

iterative reconstruction, and novel model-based iterative reconstruction algorithms, AJR. American journal of roentgenology 200(3) (2013) 545-52.
[18] A. Neroladaki, D. Botsikas, S. Boudabbous, C.D. Becker, X. Montet, Computed tomography of the chest with model-based iterative reconstruction using a radiation exposure similar to chest X-ray examination: preliminary observations, European radiology 23(2) (2013) 360-6.
[19] Y. Yamada, M. Jinzaki, T. Hosokawa, Y. Tanami, H. Sugiura, T. Abe, S. Kuribayashi, Dose reduction in chest CT: comparison of the adaptive iterative dose reduction 3D, adaptive iterative dose reduction, and filtered back projection reconstruction techniques, European journal of radiology 81(12) (2012) 4185-95.
[20] M. Katsura, I. Matsuda, M. Akahane, K. Yasaka, S. Hanaoka, H. Akai, J. Sato, A. Kunimatsu, K. Ohtomo, Model-based iterative reconstruction technique for ultralow-dose chest CT: comparison of pulmonary nodule detectability with the adaptive statistical iterative reconstruction technique, Invest Radiol 48(4) (2013) 206-12.
[21] H. MacMahon, J.H. Austin, G. Gamsu, C.J. Herold, J.R. Jett, D.P. Naidich, E.F. Patz, Jr., S.J. Swensen, Guidelines for management of small pulmonary nodules detected on CT scans: a statement from the Fleischner Society, Radiology 237(2) (2005) 395-400.
[22] D.P. Naidich, A.A. Bankier, H. MacMahon, C.M. Schaefer-Prokop, M. Pistolesi, J.M. Goo, P. Macchiarini, J.D. Crapo, C.J. Herold, J.H. Austin, W.D. Travis, Recommendations for the management of subsolid pulmonary nodules detected at CT: a statement from the Fleischner Society, Radiology 266(1) (2013) 304-17.
[23] S.K. Boone J, Cody D, McCollough CH, McNitt-Gray MF, Toth TL, Size specific dose estimates (SSDE) in pediatric and adult body CT examinations. Report of AAPM Task Group 204. , College Park: American Association of Physicists in Medicine2011.
[24] P.D. Deak, Y. Smal, W.A. Kalender, Multisection CT protocols: sex- and age-specific conversion factors used to determine effective dose from dose-length product, Radiology 257(1) (2010) 158-66.
[25] A. Huber, J. Landau, L. Ebner, Y. Butikofer, L. Leidolt, B. Brela, M. May, J. Heverhagen, A. Christe, Performance of ultralow-dose CT with iterative reconstruction in lung cancer screening: limiting radiation exposure to the equivalent of conventional chest X-ray imaging, European radiology (2016).
[26] A. Padole, S. Singh, J.B. Ackman, C. Wu, S. Do, S. Pourjabbar, R.D. Khawaja, A. Otrakji, S. Digumarthy, J.A. Shepard, M. Kalra, Submillisievert chest CT with filtered back projection and iterative reconstruction techniques, AJR. American journal of roentgenology 203(4) (2014) 772-81.
[27] Y. Kim, Y.K. Kim, B.E. Lee, S.J. Lee, Y.J. Ryu, J.H. Lee, J.H. Chang, Ultra-Low-Dose CT of the Thorax Using Iterative Reconstruction: Evaluation of Image Quality and Radiation Dose Reduction, AJR. American journal of roentgenology 204(6) (2015) 1197-202.
[28] C. Nakajo, S. Heinzer, S. Montandon, V. Dunet, P. Bize, A. Feldman, C. Beigelman-Aubry, Chest CT at a dose below 0.3 mSv: impact of iterative reconstruction on image quality and lung analysis, Acta radiologica (2015).
[29] N. Horeweg, J. van Rosmalen, M.A. Heuvelmans, C.M. van der Aalst, R. Vliegenthart, E.T. Scholten, K. ten Haaf, K. Nackaerts, J.W. Lammers, C. Weenink, H.J. Groen, P. van Ooijen, P.A. de Jong, G.H. de Bock, W. Mali, H.J. de Koning, M. Oudkerk, Lung cancer probability in patients with CT-detected pulmonary nodules: a prespecified analysis of data from the NELSON trial of low-dose CT screening, The Lancet. Oncology 15(12) (2014) 1332-41.

Tables:

Table 1. Patient characteristics for study.

Sex	M: 62 ; F:38	
Mean age (years)	66.2	(R:43-89)
Weight (kg)	81.1	± 18.3 SD
Height (cm)	170	± 9 SD
Mean BMI (kg/m2)	28.2	± 6.5 SD
≤ 20	4	
20.1-25	26	
25.1-30	38	
30.1-35	19	
35.1-40	7	
40.1-45	2	
≥ 45.1	2	
Body diameter (cm)		
Anterior Dimension	28.9	± 3.7 SD
Lateral Dimension	36.2	± 4.3 SD

Footnote: SD-standard deviation; R-Range; BMI-body mass index

Table 2. Radiation doses as per protocol

	CTDI Vol (mGy)		DLP (mGy-cm)		SSDE (mGy)		Effective Dose (mSv)	
STD	6.6	± 2.6	235.4	± 90.1	7.4	± 2.5	3.30	± 1.26
RD1	2.0	± 1.5	68.7	± 51.4	2.1	± 1.5	0.96	± 0.72
RD2	0.3	± 0.01	9.9	± 0.9	0.3	± 0.1	0.14	± 0.01

Footnote: CTDIvol-CT Dose Index Volume; DLP-Dose Length Product;

SSDE-Size-specific dose estimates; mGy-milliGray; mSv-milliSievert

STD-Standard dose; RD1-Reduced dose 1; RD2-Reduced dose 2

Table 3. Mean noise and signal-to-noise ratio across different dose and reconstruction algorithms.

	STANDARD DOSE			REDUCED DOSE 1			REDUCED DOSE 2		
	ASIR	FBP	MBIR	ASIR	FBP	MBIR	ASIR	FBP	MBIR
Mean	25.01	30.76	10.66	48.28	59.39	13.62	114.8	141.5	19.25
Std. Deviation	3.027	3.472	1.821	10.51	13.04	2.67	27.31	31.53	6.251
Std. Error	0.2886	0.331	0.1737	1.002	1.244	0.2546	2.604	3.006	0.596
Signal-to-Noise	1.55	1.26	3.44	0.81	0.66	2.76	0.34	0.29	1.29

Footnote: FBP-filtered back projection; ASIR-adaptive statistical iterative reconstruction; MBIR-model-based iterative reconstruction

Table 4. Mean attenuation values across different dose and reconstruction algorithms.

	STANDARD DOSE			REDUCED DOSE 1			REDUCED DOSE 2		
	ASIR	FBP	MBIR	ASIR	FBP	MBIR	ASIR	FBP	MBIR
Mean	38.67	38.62	36.7	38.97	38.96	37.58	38.78	40.72	24.79
Std. Deviation	7.37	7.41	6.993	10.42	10.53	10.67	18.21	18.84	15.98
Std. Error	0.7027	0.7065	0.6667	0.994	1.004	1.017	1.737	1.796	1.524

Footnote: FBP-filtered back projection; ASIR-adaptive statistical iterative reconstruction; MBIR-model-based iterative reconstruction

Table 5. Average scores of subjective image nose, image contrast and diagnostic confidence with significance testing and kappa

Subjective Image Noise

	STANDARD DOSE			REDUCED DOSE 1			REDUCED DOSE 2		
	ASIR	FBP	MBIR	ASIR	FBP	MBIR	ASIR	FBP	MBIR
Mean	4.88	4.84	4.88	4.79	4.66	4.68	4.66	4.60	4.66
Std. Deviation	0.42	0.49	0.41	0.59	0.82	0.72	0.82	0.96	0.81
Significance	control			*	*	*	*	*	*
Kappa	0.54	0.74	0.57	0.61	0.62	0.62	0.71	0.81	0.75

Subjective image noise were assessed using a five-point scale

1 = unacceptable image noise, 2 = above average noise, 3 = average image noise,

4 = less than average noise, and 5 = minimal image noise

Subjective Image Contrast

	STANDARD DOSE			REDUCED DOSE 1			REDUCED DOSE 2		
	ASIR	FBP	MBIR	ASIR	FBP	MBIR	ASIR	FBP	MBIR
Mean	4.61	4.59	4.63	4.59	3.97	4.21	3.96	3.92	4.00
Std. Deviation	0.57	0.61	0.52	0.70	0.72	0.70	0.76	0.76	0.63
Significance	control			*	*	*	*	*	*
Kappa	0.87	0.86	0.74	0.89	0.74	0.78	0.69	0.65	0.65

Image contrast were assessed by using a five-point scale

1= very poor contrast, 2 = suboptimal image contrast, 3 = acceptable image contrast,

4 = above average contrast, and 5 = excellent image contrast

Diagnostic Confidence

	0			REDUCED DOSE 1			REDUCED DOSE 2		
	ASIR	FBP	MBIR	ASIR	FBP	MBIR	ASIR	FBP	MBIR
Mean	3.88	3.90	3.81	3.54	3.49	3.65	3.24	3.23	3.25
Std. Deviation	0.32	0.30	0.39	0.53	0.54	0.48	0.70	0.78	0.68
Significance	control			*	*	*	*	*	*
Kappa	0.75	0.89	0.70	0.72	0.54	0.84	0.73	0.85	0.81

Diagnostic confidence were assessed by using a four-point scale

1 = poor confidence, 2 = confident only for a limited clinical entity such as a calcified lesion, or a large lesion,

3 = probably confident, and 4 = completely confident

* denotes statistical significance ($p<0.05$) as calculated by Friedman's test with Dunn's multiple comparison

Footnote: FBP-filtered back projection; ASIR-adaptive statistical iterative reconstruction; MBIR-model-based iterative reconstruction

Table 6. Overall sensitivity, specificity and AUC for each type of nodule

		STANDARD DOSE				REDUCED DOSE 1 (RD1)						REDUCED DOSE 2 (RD2)					
		FBP		MBIR		ASIR		FBP		MBIR		ASIR		FBP		MBIR	
		Rater 1	Rater 2	Rater 1	Rater 2	Rater 1	Rater 2	Rater 1	Rater 2	Rater 1	Rater 2	Rater 1	Rater 2	Rater 1	Rater 2	Rater 1	Rater 2
SOLID NODULES	Sensitivity	96.3	93.5	99.1	96.3	95.4	92.6	91.7	88.9	94.4	91.7	83.3	83.3	71.3	68.2	84.3	83.3
	Specificity	100	100	100	100	100	100	100	100	100	100	100	100	100	100	100	100
n = 108	AUC	0.981	0.968	0.995	0.981	0.977	0.963	0.958	0.944	0.972	0.958	0.917	0.916	0.856	0.841	0.921	0.916
SUBSOLID NODULES	Sensitivity	97.9	100.0	97.9	100.0	95.7	97.9	89.4	91.5	95.7	97.9	87.2	87.2	78.7	76.6	87.2	87.2
	Specificity	100	99.76	100	99.8	100	99.76	100	99.76	100	99.76	100	99.76	100	100	100	99.76
n = 47	AUC	0.989	0.999	0.989	0.999	0.979	0.988	0.947	0.956	0.979	0.988	0.936	0.935	0.894	0.883	0.936	0.935
PURELY CALCIFIED	Sensitivity	100.0	97.8	100.0	97.8	100.0	97.8	100.0	97.8	100.0	97.8	100.0	95.5	100.0	95.5	100.0	95.5
	Specificity	100	100	100	100	100	100	100	100	100	100	100	100	100	100	100	100
n = 89	AUC	1	0.989	1	0.989	1	0.989	1	0.989	1	0.989	1	0.978	1	0.978	1	0.978

Footnote: FBP-filtered back projection; ASIR-adaptive statistical iterative reconstruction; MBIR-model-based iterative reconstruction

Table 7. Sensitivity, specificity and AUC for solid nodules by size.

SOLID NODULES BY SIZE		STANDARD DOSE				REDUCED DOSE 1 (RD1)						REDUCED DOSE 2 (RD2)					
		FBP		MBIR		ASIR		FBP		MBIR		ASIR		FBP		MBIR	
		Rater 1	Rater 2	Rater 1	Rater 2	Rater 1	Rater 2	Rater 1	Rater 2	Rater 1	Rater 2	Rater 1	Rater 2	Rater 1	Rater 2	Rater 1	Rater 2
≤4mm	Sensitivity	91.3	87.0	95.7	91.3	87.0	82.6	82.6	78.3	87.0	82.6	43.5	43.5	21.7	17.4	47.8	47.8
n = 23	Specificity	100	100	100	100	100	100	100	100	100	100	100	100	100	100	100	100
	AUC	0.957	0.935	0.978	0.957	0.935	0.913	0.913	0.891	0.935	0.913	0.717	0.717	0.609	0.587	0.739	0.739
4.1-5.9mm	Sensitivity	94.4	91.7	100.0	97.2	94.4	91.7	86.1	83.3	91.7	88.9	91.7	88.9	80.6	72.2	91.7	88.9
n = 36	Specificity	100	100	100	100	100	100	100	100	100	100	100	100	100	100	100	100
	AUC	0.972	0.98	1	0.98	0.972	0.98	0.931	0.98	0.958	0.98	0.958	0.98	0.903	0.94	0.958	0.96
6-7.9mm	Sensitivity	100.0	96.0	100.0	96.0	100.0	96.0	100.0	96.0	96.0	96.0	92.0	96.0	88.0	88.0	92.0	92.0
n = 25	Specificity	100	100	100	100	100	100	100	100	100	100	100	100	100	100	100	100
	AUC	1	0.98	1	0.98	1	0.98	1	0.98	1	0.98	0.96	0.98	0.94	0.94	0.96	0.96
≥8mm	Sensitivity	100	100	100	100	100	100	100	100	100	100	100	100	87.5	91.3	100	100
n = 24	Specificity	100	100	100	100	100	100	100	100	100	100	100	100	100	100	100	100
	AUC	1	1	1	1	1	1	1	1	1	1	1	1	0.938	0.957	1	1

Footnote: FBP-filtered back projection; ASIR-adaptive statistical iterative reconstruction; MBIR-model-based iterative reconstruction

Table 8. Sensitivity, specificity and AUC for subsolid nodules by size

SUBSOLID NODULES BY SIZE		STANDARD DOSE				REDUCED DOSE 1 (RD1)						REDUCED DOSE 2 (RD2)					
		FBP		MBIR		ASIR		FBP		MBIR		ASIR		FBP		MBIR	
		Rater 1	Rater 2	Rater 1	Rater 2	Rater 1	Rater 2	Rater 1	Rater 2	Rater 1	Rater 2	Rater 1	Rater 2	Rater 1	Rater 2	Rater 1	Rater 2
≤5mm	Sensitivity	97.1	100.0	97.1	100.0	94.3	97.1	85.7	88.6	94.3	97.1	82.9	82.9	71.4	68.6	82.9	82.9
n = 35	Specificity	100.0	100.0	100.0	100.0	100.0	100.0	100.0	100.0	100.0	100.0	100.0	100.0	100.0	100.0	100.0	100.0
	AUC	0.986	1	0.986	1	0.971	0.986	0.929	0.943	0.971	0.986	0.914	0.914	0.857	0.843	0.914	0.914
>5.1 mm	Sensitivity	100	100	100	100	100	100	100	100	100	100	100	100	100	100	100	100
n = 12	Specificity	100.0	97.9	100.0	97.9	100.0	97.9	100.0	97.9	100.0	97.9	100.0	97.9	100.0	100.0	100.0	97.9
	AUC	1	0.99	1	0.99	1	0.99	1	0.99	1	0.99	1	0.99	1	1	1	0.99

Footnote: FBP-filtered back projection; ASIR-adaptive statistical iterative reconstruction; MBIR-model-based iterative reconstruction

Figure Legends:

Figure 1. Flow chart demonstrating scan order sequence. All patients received 3 scans in total and each scan was reconstructed with filtered-back projection (FBP), adaptive statistical iterative reconstruction (ASIR) with 30% blending, and model-based iterative reconstruction (MBIR). For each patient, this generated a total of 9 scans. Standard dose with ASIR was used as reference standard. The remaining scans and reconstruction algorithms serve as index tests under evaluation. The order of the 2 reduced dose scans were randomized after the initial standard of care scan.

Figure 2. Example of 4mm nodule in female patient with BMI 33. Despite small size, the nodules were conspicuous on all reconstruction and doses. A-STD FBP; B-STD ASIR; C-STD MBIR; D-RD1 FBP; E-RD1 ASIR; F-RD1 MBIR; G-RD2 FBP; H-RD2 ASIR; I-RD2 MBIR

Figure 3. Example of 6mm ground glass nodule in male patient with BMI 31 which were conspicuous on all reconstruction and doses but less clear on RD2. A-STD FBP; B-STD ASIR; C-STD MBIR; D-RD1 FBP; E-RD1 ASIR; F-RD1 MBIR; G-RD2 FBP; H-RD2 ASIR; I-RD2 MBIR

Figure 4. Example of 3mm solid nodule in male patient BMI 33 just barely perceptible on MBIR RD2 but not in other RD2 images. A-STD FBP; B-STD ASIR; C-STD MBIR; D-RD1 FBP; E-RD1 ASIR; F-RD1 MBIR; G-RD2 FBP; H-RD2 ASIR; I-RD2 MBIR

Figure 5. Example of 2mm solid nodule in female patient BMI 54 which was not seen on RD2. A-STD FBP; B-STD ASIR; C-STD MBIR; D-RD1 FBP; E-RD1 ASIR; F-RD1 MBIR; G-RD2 FBP; H-RD2 ASIR; I-RD2 MBIR

Figure 6. Example of several sub 4mm solid nodules in male patient BMI 52 which were less conspicuous on RD2. A-STD FBP; B-STD ASIR; C-STD MBIR; D-RD1 FBP; E-RD1 ASIR; F-RD1 MBIR; G-RD2 FBP; H-RD2 ASIR; I-RD2 MBIR

Figure 1

Click here to download high resolution image

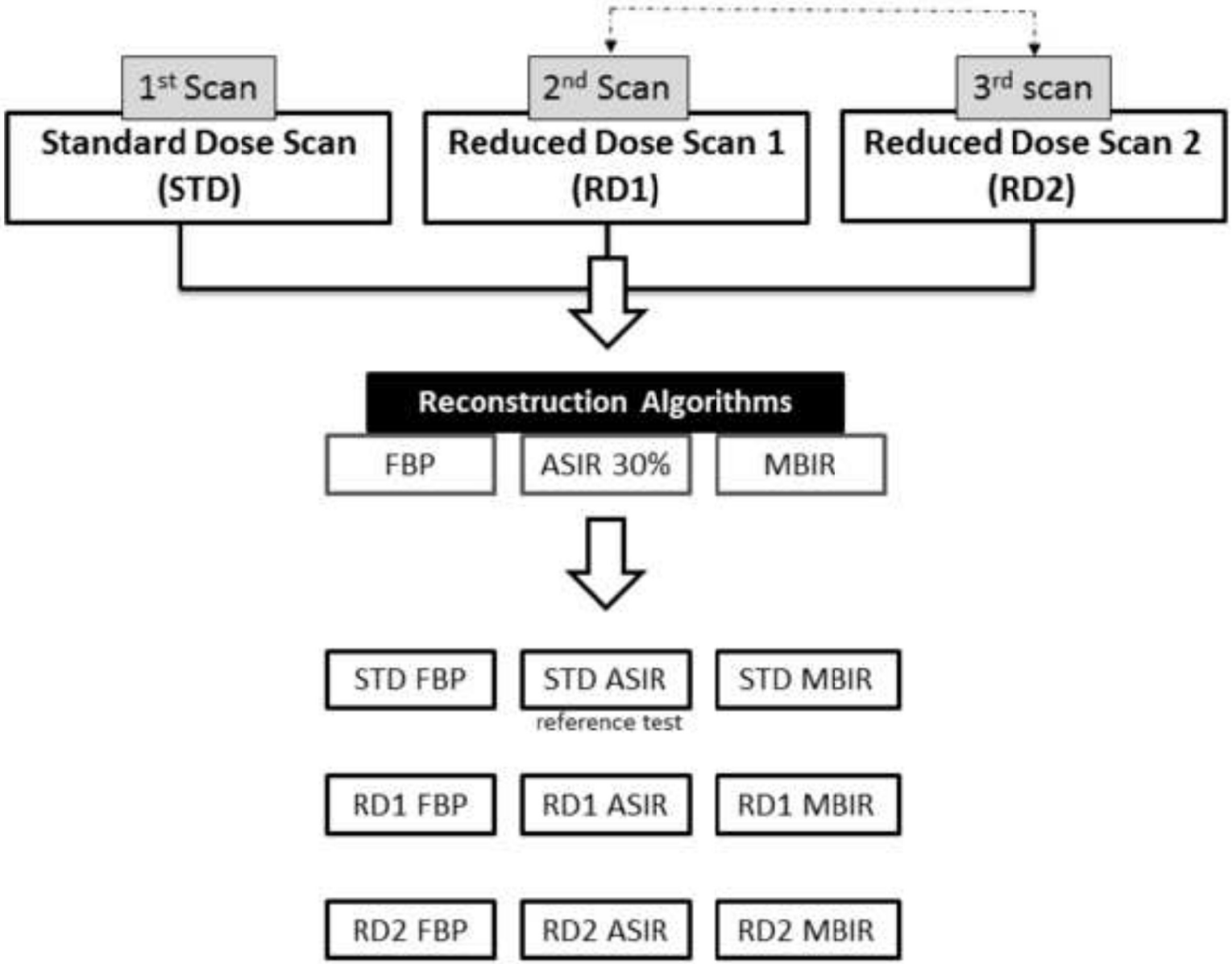

Figure 2
Click here to download high resolution image

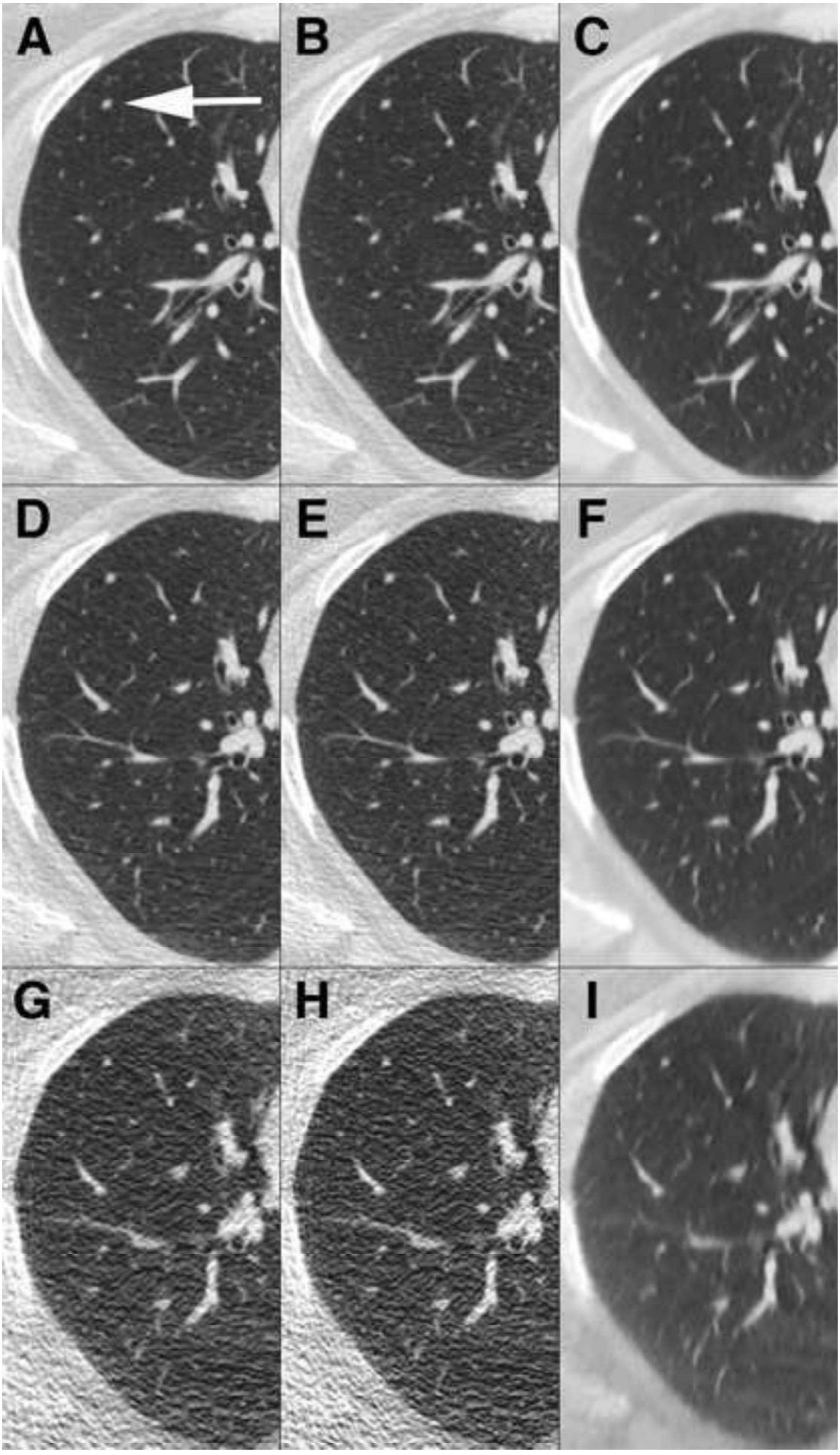

Figure 3
Click here to download high resolution image

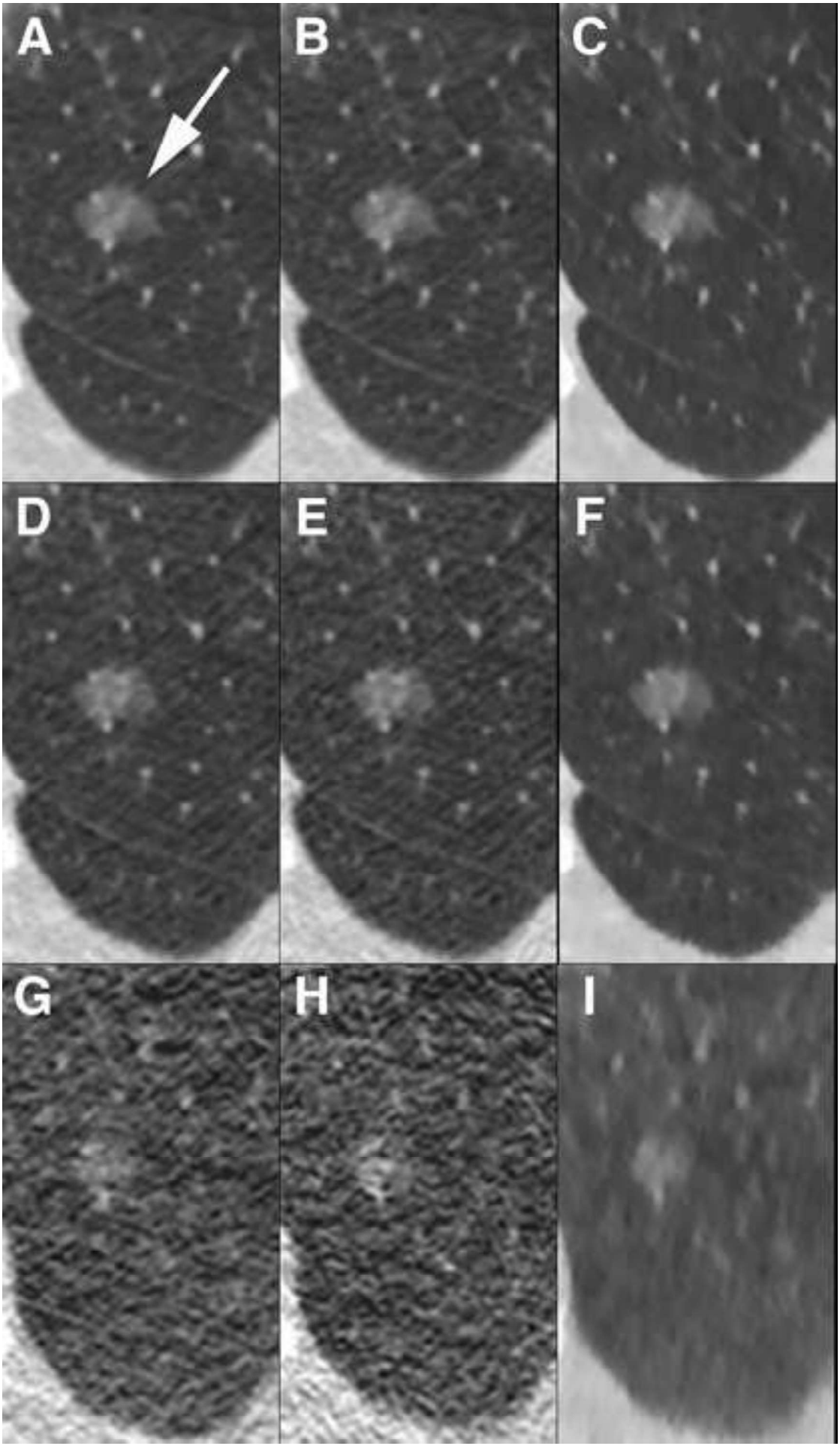

Figure 4
Click here to download high resolution image

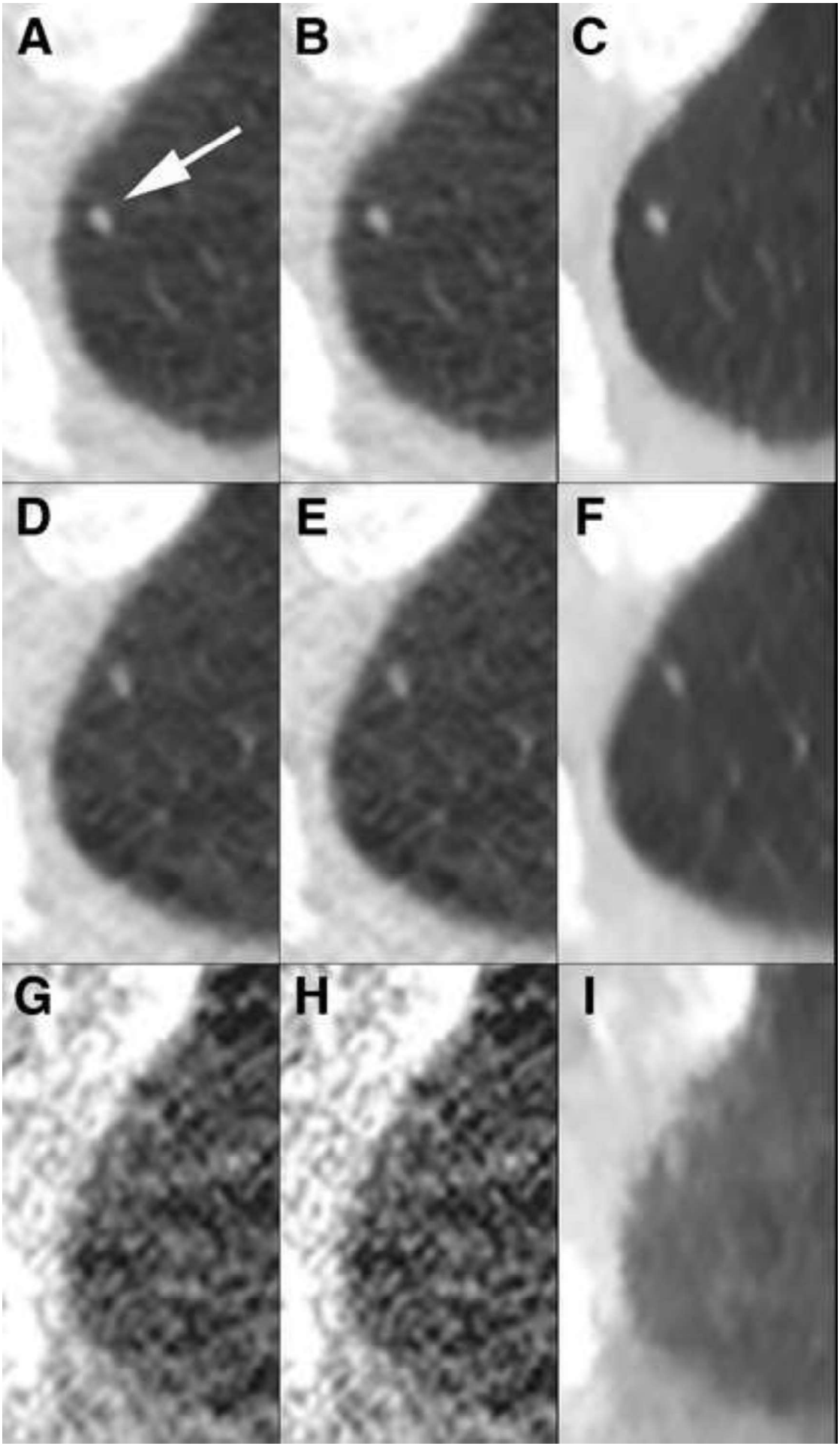

Figure 5
Click here to download high resolution image

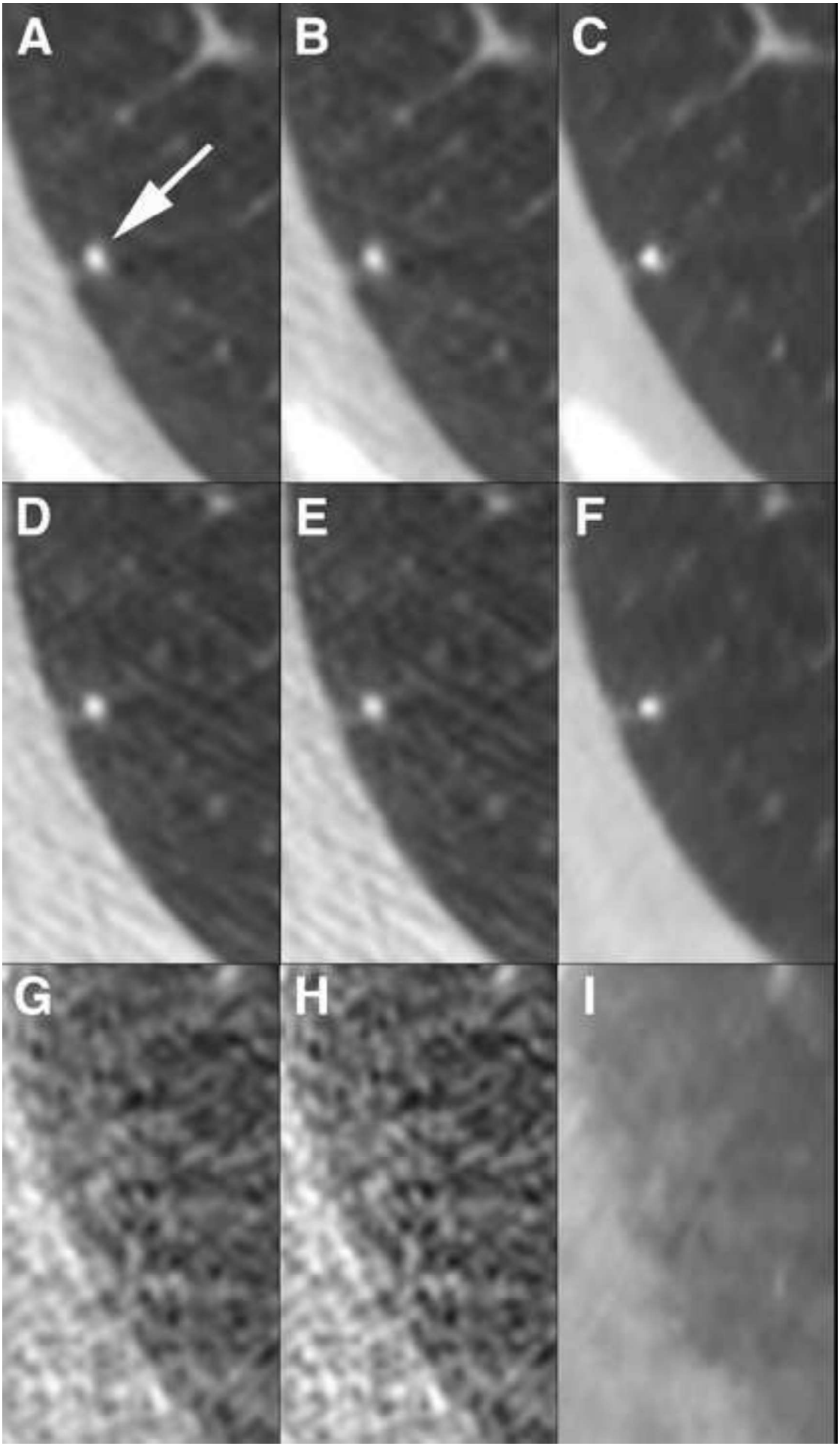

Figure 6
Click here to download high resolution image